Optimization of Multistage Olefin/Paraffin Membrane Separation Processes through Rigorous Modeling

Authors: Raúl Zarca[1], Alfredo Ortiz[1], Daniel Gorri[1], Lorenz T. Biegler[2], Inmaculada Ortiz[1]*.

[1]Dept. of Chemical and Biomolecular Engineering. University of Cantabria, Av. Los Castros 46, 39005 Santander, Spain

[2]Dept. of Chemical Engineering, Carnegie-Mellon University, 5000 Forbes Avenue, Pittsburgh, PA 15213

*corresponding author: ortizi@unican.es

Revised Manuscript

Submitted to AIChE Journal

February 2019

Abstract

In this work, we explore the capabilities of an NLP optimization model to determine the viability of facilitated transport membrane processes intended to replace traditional distillation currently employed for propane/propylene separation. An NLP optimization model for multistage membrane processes has been formulated, introducing the mathematical description of the facilitated transport mechanisms in the PVDF-HFP/BMImBF$_4$/AgBF$_4$ membranes previously developed by our research group. For the first time, a simultaneous optimization of the process and the membrane material (i.e. carrier concentration) has been performed, thanks to the implementation of the governing equations for the fixed site and mobile carrier mechanisms. Once the model is solved in GAMS it returns the optimal membrane area, carrier loading and permeate pressure of each stage based on Net Present Value Cost (NPVC) minimization. Different process flowsheets were evaluated and the results show prominent reductions on NPVC for facilitated transport multistage processes when compared to distillation.

Introduction

Propane/propylene gaseous mixtures resulting from fluid catalytic cracking and steam cracking are commonly separated using high pressure or cryogenic distillation, which is associated to major energy and capital consumptions.[1] Through the last years, process intensification by means of membrane technology has emerged as a promising alternative to large, expensive and energy-intensive distillation units.[2]

Many membrane materials have been reported for olefin/paraffin separation, including polymers,[3–5] and more complex materials, such as carbon molecular sieves (CMSs),[6–9] zeolitic imidazolate frameworks (ZIFs)[10–14] or facilitated transport membranes.[15,16] Among these, facilitated transport membranes can easily surpass the permeability-selectivity trade-off of polymeric membranes thanks to the reversible reaction between the olefin and a carrier cation, typically silver, which is added to the membrane composition.[17,18] Facilitated transport membranes have been synthesized following different approaches, from supported liquid membranes (SLM)[19,20] to supported ionic liquid membranes (SILM)[21] that replace organic solvents with non-volatile room temperature ionic liquids (RTILs)[22] in order to avoid solvent losses through evaporation.[23] Recently, composite facilitated transport membranes prepared by solvent casting of a polyvinylidene fluoride-hexafluoropropylene (PVDF-HFP) polymeric solution containing the ionic liquid and the silver salt have been reported.[24] In these dense membranes, which feature a combination of fixed site and mobile carrier transport mechanisms,[25] selectivities up to 150 and propylene permeabilities higher than 1000 Barrer have been achieved that avoid the issues of supported liquid membranes.

Since a single-stage membrane process that produces polymer grade propylene and fuel grade propane simultaneously is only feasible for high concentrated feeds [26], due to the purity-recovery trade-off inherent in membrane operation, the implementation of membrane technology to intensify the olefin/paraffin separation process can be carried out according to two different approaches. The first one involves the use of membrane modules along with new or existing distillation columns to create a hybrid process that reduces the required reflux ratio and its associated expenses.[27–31] The second approach achieves complete replacement of the distillation column with membrane technology by designing and optimizing appropriate multistage/multistep membrane processes.[32,33]

In particular, several trade-offs should be balanced when designing a multistage membrane process based on facilitated transport membranes. Firstly, the total membrane area of each stage determines the flowrates and purities of the product streams in that stage. Thus, higher stage areas generate larger permeate flowrates at the expense of permeate purity. In addition, the transmembrane flux of the transported species in these membranes is strongly dependent on the carrier loading, as derived from the experimental analysis and the mathematical models.[21,25] However, high carrier concentrations imply high membrane cost per unit area, which could affect the process economics. Finally, higher transmembrane pressures increase the available driving force for the permeation but at the expense of higher recompression requirements.

Moreover, the whole process flowsheet can be optimized in order to obtain the optimal process configuration in terms of number of stages, mixers, splitters and compressors. This type of optimization involves the design of superstructures that are solved using

binary variables, which result in complex mixed integer nonlinear programming problems "MINLP".[34] In this regard, the works by Prof. Agrawal's group provide extensive insight on this design strategy. [35,36] However, MINLP problems are difficult to solve because they combine challenges of nonlinear and mixed integer programming, and require dedicated methods for its resolution.[37] Instead, while it is often possible to study all potential multistage configurations in one single superstructure, most studies dealing with superstructure optimization for membrane separation show that in many cases a two-stage configuration is optimal.[38–40]

Therefore, in this work we focus on the optimization of the implicit trade-offs in two multistage facilitated transport processes, specifically, one conventional two-stage configuration and one two-stage configuration with a two-step second stage, commonly known as "two-and-one-half" stage process.[32] In this manner, the complex mixed-integer nonlinear formulations associated to superstructures can be replaced with a nonlinear programming problem. The membrane modules have been modelled as hollow fiber modules, which is the most adequate configuration for gas separation, featuring high packing densities and energy efficiency.[41–44] Furthermore, the mass balances in the membrane modules have been described as ordinary differential equations and have been solved using orthogonal collocation on finite elements.[45] Consequently, black box modeling approaches can be avoided, thus allowing the study of the transmembrane flux profiles along the fibers. These profiles will show how the optimization works in balancing the recovery-purity trade-off by varying the membrane total area of each stage. Additionally, a simultaneous optimization of the process and

the membrane material (i.e. carrier load) has been possible thanks to the introduction of the equations that govern the facilitated transport mechanisms.[25] To the best of our knowledge, this is the first time that this joint optimization is performed without solving an upper-bound type equation for the selectivity-permeability trade-off, whose solution does not necessarily represent a real membrane material.[46] Finally, the objective function accounts for the process economics, which assesses the potential of facilitated transport multistage processes to replace current distillation.

Theoretical Background

Single-Stage and Multistage Membrane Processes

In membrane process design the basic unit is the membrane stage, which can be defined as an operating unit, comprising one or more membrane modules, which performs a specific task different from any other membrane stages existing in the same process. A single-stage process, shown in Figure 1, is the simplest membrane process that can be designed, although some major limitations in membrane operations affect these processes. In particular, membrane material selectivity and the industrially reachable pressure ratio prevent satisfying high product purity and recovery simultaneously, and process engineers may have to sacrifice one of these specifications. Therefore, single-stage processes are often used for bulk concentration prior to further purification processes.[47]

To overcome the limitations of single-stage membrane processes more stages could be interconnected, generating different multistage configurations. Staging a membrane process involves solving the trade-off between capital expenses (additional compressors and membrane modules) and product recovery. Although there are many multistage configurations, the two-stage and the so-called two-and-one-half stage processes,[48] are preferred over three stage or higher multistage processes.[32] In the two-stage process, shown in Figure 2, the recompressed permeate of the first stage is fed into a second stage for a further purification step. The retentate of the second stage is then recycled and mixed with the original feed. Another usual two-stage variation uses the retentate of

the first stage as feed for the second stage. However, such configuration is commonly used when the retentate is the final product and the purity of the more permeant species is not a concern.[32]

In comparison, the two-and-one-half process shown in Figure 3 uses a two-step separation for the second stage and the permeate stream of the second step is recycled to the first step feed. This configuration can achieve any desired concentration of the more permeable gas by controlling the relative size of the second stage modules. Moreover, to balance the tradeoffs and calculate the feed and permeate pressures and the membrane area of each stage, process optimization is required.

Discretized membrane model

Previous studies on membrane process optimization usually make use of simplified membrane models. These shortcut models are typically implemented within superstructures that are solved as mixed-integer optimization problems.[38] For processes where a more detailed description of the membrane separator is needed as in the case of hollow fibers modules, a perfect cross-flow model is usually employed. This model assumes plug-flow in the high pressure side of the fiber, usually the lumen side, and perfect mixed flow in the permeate side, i.e. shell side.[28] However, assuming that the feed flows through the lumen side may seem unrealistic in gas separation hollow fibers, whereby the active layer is often formed in the outer fiber surface. In addition, most membrane models assume fixed permeability/selectivity values for a given membrane material. In contrast, the rigorous facilitated transport model used in this work requires

calculating the partial pressure profiles along the module. To address these issues, a fully discretized optimization model has been developed in this work.

The membrane model is depicted in Figure 4 and is based on the following assumptions:

- The feed and permeate streams flow through the shell and lumen sides of the fibers respectively.

- The module operates isothermally and in steady state.

- The feed and permeate streams flow in co-current mode.

- Plug-flow is assumed at both sides of the membrane.

- The total feed and permeate pressures are operation constants.

- The only pressure drop in the membrane module is the transmembrane pressure.

The component molar flowrates are discretized according to the following mass balances:

$$dF_j^F(z) = -J_j(z) \cdot dA \qquad (1)$$

$$dF_j^P(z) = J_j(z) \cdot dA \qquad (2)$$

where F_j and J_j are the molar flowrate and the transmembrane flux of component j, respectively, and dA is the fiber outer wall area differential element. The dimensionless fiber axial length is defined as:

$$\bar{z} = \frac{z}{L} \qquad \bar{z} \in [0,1] \tag{3}$$

where L is the total fiber length. Rearranging terms, the mass balances (ODEs) and the boundary conditions can now be rewritten as:

$$\frac{dF_j^F(\bar{z})}{d\bar{z}} = -J_j(\bar{z}) \cdot A_{Total} \tag{4}$$

$$\frac{dF_j^P(\bar{z})}{d\bar{z}} = J_j(\bar{z}) \cdot A_{Total} \tag{5}$$

$$F_j^F|_{\bar{z}=0} = F_j^F(\bar{z} = 0) \tag{6}$$

$$F_j^P|_{\bar{z}=1} = F_j^P(\bar{z} = 1) \tag{7}$$

One of the main features of this work is that the membrane material optimization (i.e. carrier concentration) and the multistage process optimization are performed simultaneously. For this purpose, the rigorous facilitated transport model previously developed by this research group has been implemented in the optimization,[25] particularly for PVDF-HFP/BMImBF$_4$/AgBF$_4$ membranes containing silver as carrier. In this model, which was specifically developed for facilitated transport membranes that combine fixed and mobile carrier mechanisms, the permeability of the paraffin can be considered constant. Thus its transmembrane flux is described through the solution-diffusion model:[49]

$$J_{C_3H_8}(\bar{z}) = \frac{P_{C_3H_8}}{\delta} \left[p_{C_3H_8}^F(\bar{z}) - p_{C_3H_8}^P(\bar{z}) \right] \tag{8}$$

where $P_{C_3H_8}$ is the paraffin permeability, δ is the active layer thickness and $p_{C_3H_8}^F$ and $p_{C_3H_8}^P$ are the feed and permeate partial pressure of the paraffin.

Conversely, the olefin flux, i.e. the preferentially transported species, is affected by the complexation reaction with the silver cations:

$$[Ag^+] + C_3H_6 \overset{k_{eq}}{\Longleftrightarrow} Ag^+(C_3H_6) \tag{9}$$

The flux can be calculated as the sum of the contributions of three transport mechanisms: solution-diffusion, fixed-site carrier and mobile carrier:

$$J_{C_3H_6}(\bar{z}) = J_{C_3H_6,SD}(\bar{z}) + J_{C_3H_6,MC}(\bar{z}) + J_{C_3H_6,FC}(\bar{z}) \tag{10}$$

$$J_{C_3H_6,SD}(\bar{z}) = D_{C_3H_6,m} \cdot S_{C_3H_6,m} \frac{p_{C_3H_6}^F(\bar{z}) - p_{C_3H_6}^P(\bar{z})}{\delta} \tag{11}$$

$$J_{C_3H_6,MC}(\bar{z}) = \frac{k_{eq} \cdot [Ag^T] \cdot H_{C_3H_6}}{1 + k_{eq} \cdot p_{C_3H_8}^P(\bar{z}) \cdot H_{C_3H_6}} D_{comp} \frac{p_{C_3H_6}^F(\bar{z}) - p_{C_3H_6}^P(\bar{z})}{\delta} x_{IL} \tag{12}$$

$$J_{C_3H_6,FC}(\bar{z}) = K_{FC}(\bar{z}) \cdot \frac{p_{C_3H_6}^F(\bar{z}) - p_{C_3H_6}^P(\bar{z})}{\delta} (1 - x_{IL}) \tag{13}$$

$$K_{FC}(\bar{z}) = \alpha \left(\frac{[Ag^T]}{1 + k_p p_{C_3H_6}^P(\bar{z})} \right) \tag{14}$$

where k_{eq} is the complexation constant, $H_{C_3H_6}$ is the propylene solubility in the composite membrane, x_{IL} is the ionic liquid mass fraction in the membrane composition, α is a fitting parameter for the fixed-site carrier mechanism and $[Ag^T]$ is the silver concentration in the membrane. The temperature dependencies have been

omitted as isothermal operation has been assumed. The contribution of the Fickian diffusion to the olefin transmembrane flux (Eq.11) is negligible compared to the contribution of the facilitated transport mechanisms (Eq. 12-13) and, in consequence, it has not been included in the optimization. A detailed description of the model can be found in the original source.[25] Table 1 shows the values of the model parameters.

As commented before, the use of this specific model for facilitated transport avoids using a fixed permeability parameter and introduces carrier concentration as a decision variable. In this way, the membrane material and the multistage process can be optimized at the same time.

Finally, the ordinary differential equations (Eqs 4-7) are solved as algebraic equations after discretization through implicit Runge-Kutta collocation methods using 100 finite elements and 3 internal collocation points.

Optimization details

The aim of this work is to optimize two multistage membrane processes: a) a two-stage and b) a two-and-one-half stage, intended to produce polymer grade propylene, and enriched propane, from a C_3 refinery stream minimizing the Net Present Value Costs (NPVC) of both configurations. The feed stream is considered to come from the partial condenser of a depropanizer column. In this manner a vapor stream would be available without further processing. The pressure, temperature and composition of the original feed, stream *F* in Figures 1-3, are fixed by common refinery specifications.[50] Table 2

displays the properties of the propylene/propane mixed stream, the target product purities and the process constants and constraints.

The decision variables of the model are:

- The membrane area of each module.

- The carrier concentration of each membrane.

- The permeate pressure.

The mathematical standard form of the optimization problem can be described as:

$$Minimize\ NPVC(v)$$
$$s.t.$$
$$h(v) = 0 \tag{15}$$
$$t(v) \geq 0$$
$$U' \leq v \leq U''$$

where v is the vector of decision variables, $h(v)$ represents the set of model algebraic equations, $t(v)$ is the set of constraints (Eqs. 16-17) and U' and U'' are the lower and upper limits of the decision variables, respectively.

$$x_{C_3H_6} \geq x_{C_3H_6,min} \tag{16}$$

$$x_{C_3H_8} \geq x_{C_3H_8,min} \tag{17}$$

Finally, the objective function (NPVC) has been calculated as a combination of OPEX and CAPEX, correcting the operating expenses according to the time value of money:

$$NPVC = CAPEX + OPEX \cdot (1 - (1 + r)^{-T})/r \tag{18}$$

The parameters and constants used are shown in Table 3. A detailed description of the economic calculations can be found in a previous work.[51] Briefly, the compressor expenses have been calculated according to the *Guthrie's Modular Method for Costing and Sizing* [52] and the membrane cost is calculated using the market prices for its constituents and the optimized composition. To maintain a conservative estimation of the membrane cost, the lab-scale price of its constituents has been considered:

$$MCA = \delta \cdot (PL \cdot PP + ILL \cdot ILP + [Ag^T] \cdot M_{Ag} \cdot AGP) \qquad (19)$$

where MCA is the membrane cost per unit area, δ is the membrane thickness and M_{Ag} is the molar mass of AgBF$_4$. The membrane replacement cost has been introduced through a membrane replacement factor (MR), which is estimated as a percentage of the membrane capital cost.

The detailed equations used to assess the process economics are outlined in Appendix A. The optimization model renders a NLP problem solved in GAMS using as solver the multi-start heuristic algorithm OQNLP on a 3.40 GHz Intel® Core™ i7–3770 processor. The model statistics are detailed in Table 4. The model is solved in less than 0.1 seconds when CONOPT is used as local solver for OQNLP. The reported results are typically obtained in 500 to 1500 iterations depending on the complexity of each case.

Results and Discussion

This section presents and discusses the main results regarding the design and optimization of the proposed flowsheets. The feed stream to both flowsheets consists of

an equimolar propane/propylene mixture and the objective is to obtain propylene and propane purities of 99.5 mol% and 95 mol% respectively. The Net Present Value Cost (NPVC) of both multistage processes will be compared with the NPVC of the reference distillation column. Heat integration strategies are not considered in the distillation base case, as they heavily rely on the specific layout of each olefin production unit.

Multistage membrane process optimization results

The optimized two stage flowsheet is displayed in Figure 5. The optimal design comprises two membrane stages showing considerable size differences. The first stage requires around 14000 m^2 of membrane area to generate a propylene depleted retentate stream, thus achieving the desired propane purity. However, the second stage area is almost ten times smaller and is intended to produce a high purity propylene permeate regardless of the retentate purity.

Regarding the optimal carrier loading, its value is allowed to vary between the experimentally studied range from 0 to 6 M, where 0 M implies no facilitated transport and 6 M is the highest concentration assessed for PVDF-HFP/BMImBF$_4$/AgBF$_4$ membranes. Eventually, the optimization balances the cost-performance trade-off of the first stage at 2.33 M Ag$^+$, far below the upper limit. Since higher concentrations of carrier result in high membrane prices per unit area, this decreased optimal value helps to reduce the expenses caused by the large size of this stage. On the other hand, the second stage carrier loading hits the highest allowed level of 6 M Ag$^+$, which is consistent with the purity-oriented nature of this stage. Although the high carrier

loading of the second stage raises the membrane specific cost to 324 $/m^2, the relative small size of this stage dampens the total membrane cost.

Finally, it should be noted that this multistage configuration generates a large reflux stream with high associated compression costs. Nonetheless, the optimal permeate pressure of both stages falls to 1 bar, promoting higher driving force in the modules at the expense of higher compression duty.

In order to gain better insight on the optimal stage design, the transmembrane flux profiles along the fiber modules have been calculated. Figure 6 displays the propylene and propane transmembrane flux along the dimensionless axial length in each membrane stage. As it can be observed in Figure 6A the propylene transmembrane flux of stage M1 starts at a high level ($\sim$6x10^{-3} mol m^{-2} s^{-1}) thanks to the facilitated transport mechanisms and the significant driving force achieved in the hollow fibers. The resulting high permeation flux in combination with the large membrane area depletes the propylene concentration of the retentate stream and, eventually, its driving force falls until the transmembrane flux of propane ($\sim$6x10^{-4} mol m^{-2} s^{-1}) exceeds that of the propylene. The optimal solution involves continuing the operation past that point to be able to generate the optimal cut-off. Figure 7 shows the molar fractions of propane and propylene in the retentate and permeate streams. In contrast, Figure 6B shows the same profiles in stage M2, but in this case the propylene transmembrane flux remains almost constant due to the reduced membrane area required, which produces a polymer grade propylene stream as permeate but maintains a notable propylene concentration in the retentate.

This is a good example of how optimization can solve the intrinsic tradeoff between productivity and purity, and displaces it towards high permeate volume production or high product purity depending on the specific task of each stage within the multistage process.

The "two-and-one-half stage" process optimization results are shown in Figure 8. The main feature of this process is the introduction of a third stage intended to recycle a propylene enriched stream back to the second stage feed, in this manner the outer loop recycle is reduced, minimizing the total membrane area requirements in the stage M1 and the subsequent compression duty. As in the two stage process, the first stage (M1) is significantly larger than the next stages (M2 and M3) and its optimal carrier concentration is below the upper bound, at 2.30 M Ag^+. Again, the M2 and M3 stages require the maximum carrier loading of 6 M Ag^+, which increases the membrane performance at the expense of higher membrane costs. However, although the introduction of a third stage helps to minimize the compression requirements by decreasing the recycle flowrate, this reduction is not significant enough and may not justify its implementation. This can be observed by the relative small size of stage M3, which is almost negligible compared with the other stages. The optimization results of both processes are detailed in Table 5.

It should be noted that the optimal permeate pressure in both case studies and in all stages falls to 1 bar. Although the compression is a capital-intensive operation, the permeate pressure has a major influence on the objective function. A higher permeate pressure reduces the available driving force for the permeation, which involves larger

membrane areas and a higher recycle flowrate. In this manner, the reduction in the required recompression does not produce any savings, because the potential benefits are hindered by the large flowrate that needs to be recompressed and the CAPEX associated to extra membrane area.

A brief analysis of the transmembrane flux profiles in the "two-and-one-half" stage process reveals similar design criteria as in the first studied case. Figure 9A-C displays the propylene and propane transmembrane flux along the dimensionless axial length of the fibers module.

As commented before, the large membrane area required in the first stage is intended to achieve the desired propane purity in one single pass. As a result, most of the propylene permeates and its driving force is reduced until its transmembrane flux falls below the propane level, see Figure 9A. Notice that this is not detrimental when the product stream is the retentate, as is the case for stage M1. However, the subsequent stages, Figures 8B-C, are intended to produce a propylene-enriched permeate and consequently, the propylene transmembrane flux remains high along the fiber modules, thanks to the relatively small areas involved in these stages.

NPVC comparison

The NPVC of both membrane processes and the base case distillation are itemized in Table 6. The results reveal the prominent potential of facilitated transport membrane processes to replace the traditional distillation and to sharply decrease the investment

expenses when implementing the two stage membrane process. On the other hand, the introduction of an additional separation step in the "two-and-one-half" stage flowsheet produces minor savings compared to the two stages process and, therefore, a less complex process may be preferred. It is worth noting that the main difference between the base case distillation and the membrane processes is not in the capital expenses but in the operating costs, which is consistent with the use of process steam in the distillation reboiler. As expected, process intensification through membrane technology plays here a major role in energy saving.

The cost data included in Table 6 for the distillation column correspond to the base case reported in our previous paper,[29] that is, for a distillation column without heat integration. However, OPEX could be overestimated since the distillation columns can be heat integrated. Calculations reported in the literature show that heat-pump based heat-integrated columns (also known as vapor recompression design) are capable of achieving up to 75% energy savings.[14, 26, 53] Those same studies note that such designs are not routinely employed due to operational and control challenges. Instead, heat-integration can be implemented through other parts of the plant generating extra amount of low-grade heat, such as, quench water.[14] A detailed heat-integration study for distillation columns is beyond the scope of this study, since it would require analyzing the complete process flowsheet where the C3 splitter is included. However, our estimates show that even for a 50% heat-integrated column (i.e., with 50% of the reboiler duty provided by heat-integration), our proposed separation process with

membrane modules can achieve savings in energy requirement over heat-integrated distillation.

Comparison for an Extreme Purity Specification

Although propylene purities higher than 99.5% are not demanded by the polypropylene industry, it is instructive to consider a final comparison between the two-stage and two-and-half stage optimization models. For a propylene permeate specification of 99.9% we observe that the two stage process becomes infeasible and has no solution. In contrast, the two-and-half stage model is able to obtain any permeate concentration, and consequently satisfies this specification. As shown in Table 7, the optimum for this process is achieved at a much higher cost, with more than double the NPVC.

Conclusions

The complete replacement of propane/propylene distillation processes by membrane technology strongly relies on adequate membrane processes and materials design. In this work, the simultaneous optimization of multistage processes and facilitated transport membrane composition reveals potential Net Present Value Cost reductions of around 45% compared to the standalone distillation. Additionally, the optimization results showed minor differences between the two studied multistage processes. Thus, the simpler two-stage layout may be more adequate in a real scenario. Furthermore, full discretization of the model reveals how the recovery-purity trade-off and the position of

each stage within the multistage flowsheet affect the transmembrane flux profiles along the modules. In this sense, this work outlines the importance of previous mathematical modeling of transport phenomena as valuable foundations for further computer aided process engineering. Finally, future in-depth optimization works on specific olefin production plants should also consider heat integration in the benchmark distillation and product phase change in the membrane process, as it might alter the potential advantages of membrane multistage processes.

Acknowledgments

Notation

A membrane effective area [m^2]

D diffusion coefficient [$m^2 s^{-1}$]

F molar flowrate [$mol\ s^{-1}$]

H Henry's solubility constant [$mol\ bar^{-1}\ m^{-3}$]

h set of model algebraic equations

J molar transmembrane flux [$mol\ m^{-2}\ s^{-1}$]

K_{eq} equilibrium constant [$m^3\ mol^{-1}$]

K_{FC} fixed carrier effective permeability [$mol\ bar^{-1}\ m^{-1}\ s^{-1}$]

K_p heterogeneous equilibrium constant [bar^{-1}]

L fiber length [m]

P permeability [$mol\ bar^{-1}\ m^{-1}\ s^{-1}$]

p pressure [bar]

R universal gas constant [$8.314\ J\ mol^{-1}\ K^{-1}$]

r investment rate [%]

S gas solubility in the membrane [$mol\ bar^{-1}\ m^{-3}$]

T investment period [y]

t set of model constraints

U' lower limit of the decision variables

U" upper limit of the decision variables

x molar fraction [-]

x_{IL} ionic liquid mass fraction [-]

z hollow fiber axial dimension [m]

Greek letters

α fitting parameter

δ active layer thickness [m]

Superscript / subscript

0 feed side

C_3H_6 propylene

C_3H_8 propane

comp organometallic complex

FC fixed-site carrier

IL ionic liquid

L permeate side

m membrane

MC mobile carrier

r reaction

SD solution-diffusion

Literature Cited

1. Sholl DS, Lively RP. Seven chemical separations to change the world. Nature. 2016; 532:435-437.

2. Charpentier JC. In the frame of globalization and sustainability, process intensification, a path to the future of chemical and process engineering (molecules into money). Chem Eng J. 2007;134(1-3):84-92.

3. Faiz R, Li K. Polymeric membranes for light olefin/paraffin separation. Desalination. 2012;287:82-97.

4. Staudt-Bickel C, Koros WJ. Olefin/paraffin gas separations with 6FDA-based polyimide membranes. J Memb Sci. 2000;170(2):205-214.

5. Alghunaimi F, Ghanem B, Alaslai N, Mukaddam M, Pinnau I. Triptycene dimethyl-bridgehead dianhydride-based intrinsically microporous hydroxyl-functionalized polyimide for natural gas upgrading. J Memb Sci. 2016;520:240-246.

6. Xu L, Rungta M, Brayden MK, et al. Olefins-selective asymmetric carbon molecular sieve hollow fiber membranes for hybrid membrane-distillation processes for olefin/paraffin separations. J Memb Sci. 2012;423-424:314-323.

7. Liu J, Liu Y, Kayrak Talay D, Calverley E, Brayden M, Martinez M. A new carbon molecular sieve for propylene/propane separations. Carbon N Y. 2015;85:201-211.

8. Ma X, Lin YS, Wei X, Kniep J. Ultrathin carbon molecular sieve membrane for propylene/propane separation. AIChE J. 2016;62(2):491-499.

9. Salinas O, Ma X, Litwiller E, Pinnau I. High-performance carbon molecular sieve membranes for ethylene/ethane separation derived from an intrinsically microporous polyimide. J Memb Sci. 2016;500:115-123.

10. Kwon HT, Jeong HK, Lee AS, An HS, Lee JS. Heteroepitaxially grown zeolitic imidazolate framework membranes with unprecedented propylene/propane separation performances. J Am Chem Soc. 2015;137(38):12304-12311.

11. Liu D, Ma X, Xi H, Lin YS. Gas transport properties and propylene/propane separation characteristics of ZIF-8 membranes. J Memb Sci. 2014;451:85-93.

12. An H, Park S, Kwon HT, Jeong HK, Lee JS. A new superior competitor for exceptional propylene/propane separations: ZIF-67 containing mixed matrix membranes. J Memb Sci. 2017;526:367-376.

13. Da Silva FA, Rodrigues AE. Propylene/propane separation by vacuum swing adsorption using 13X zeolite. AIChE J. 2001;47(2):341-357.

14. Ma X, Kumar P, Mittal N, et al. Zeolitic imidazolate framework membranes made by ligand-induced permselectivation. Science 2018;361:1008-1011.

15. Faiz R, Li K. Olefin/paraffin separation using membrane based facilitated transport/chemical absorption techniques. Chem Eng Sci. 2012;73:261-284.

16. Yoon Y, Won J, Kang YS. Polymer electrolyte membranes containing silver ion for facilitated olefin transport. Macromolecules. 2000;33(9):3185-3186.

17. Nymeijer K, Visser T, Brilman W, Wessling M. Analysis of the complexation reaction between Ag+ and ethylene. Ind Eng Chem Res. 2004;43(11):2627-2635.

18. Rungta M, Zhang C, Xu L, Koros WJ. Membrane-based ethylene/ethane separation: The upper bound and beyond. AIChE J. 2013;59(9):3475-3489.

19. Duan S, Ito A, Ohkawa A. Separation of propylene/propane mixture by a supported liquid membrane containing triethylene glycol and a silver salt. J Memb Sci. 2003;215(1-2):53-60.

20. Ravanchi MT, Kaghazchi T, Kargari A. Supported liquid membrane separation of propylene-propane mixtures using a metal ion carrier. Desalination. 2010;250(1):130-135.

21. Fallanza M, Ortiz A, Gorri D, Ortiz I. Experimental study of the separation of propane/propylene mixtures by supported ionic liquid membranes containing Ag+–RTILs as carrier. Sep Purif Technol. 2012;97:83-89.

22. Ortiz A, Ruiz A, Gorri D, Ortiz I. Room temperature ionic liquid with silver salt as efficient reaction media for propylene/propane separation: Absorption equilibrium. Sep Purif Technol. 2008;63(2):311-318.

23. Teramoto M, Matsuyama H, Yamashiro T, Katayama Y. Separation of ethylene from ethane by supported liquid membranes containing silver-nitrate as a carrier. J Chem Eng Japan. 1986;19:419-424.

24. Fallanza M, Ortiz A, Gorri D, Ortiz I. Polymer-ionic liquid composite membranes for propane/propylene separation by facilitated transport. J Memb Sci. 2013;444:164-172.

25. Zarca R, Ortiz A, Gorri D, Ortiz I. Generalized predictive modeling for facilitated transport membranes accounting for fixed and mobile carriers. J Memb Sci. 2017;542:168-176.

26. Lee U, Kim J, Seok Chae I, Han C. Techno-economic feasibility study of membrane based propane/propylene separation process. Chem Eng Process - Process Intensif. 2017;119:62-72.

27. Kookos IK. Optimal design of membrane/distillation column hybrid processes. Ind Eng Chem Res. 2003;42(8):1731-1738.

28. Caballero JA, Grossmann IE, Keyvani M, Lenz ES, Square N, Pennsyl V. Design of hybrid distillation - vapor membrane separation systems. Ind Eng Chem Res. 2009;48:9151-9162.

29. Zarca R, Ortiz A, Gorri D, Biegler LT, Ortiz I. Optimized distillation coupled with state-of-the-art membranes for propylene purification. J Memb Sci. 2018;556:321-328.

30. Tula AK, Befort B, Garg N, Camarda K V., Gani R. Sustainable process design & analysis of hybrid separations. Comput Chem Eng. 2017;105:96-104.

31. Pressly TG, Ng KM. A break-even analysis of distillation-membrane hybrids. AIChE J. 1998;44(1):93-105.

32. Baker RW. Membrane Technology and Applications, chapter 8, 3rd edition. Chichester: Wiley; 2012.

33. Ahmad F, Lau KK, Shariff AM, Murshid G. Process simulation and optimal design of membrane separation system for CO2 capture from natural gas. Comput Chem Eng. 2012;36(1):119-128.

34. Qi R, Henson MA. Membrane system design for multicomponent gas mixtures via mixed-integer nonlinear programming. Comput Chem Eng. 2000;24(12):2719-2737.

35. Agrawal R, Xu J. Gas-separation membrane cascades utilizing limited numbers of compressors. AIChE J. 1996;42(8):2141-2154.

36. Pathare R, Agrawal R. Design of membrane cascades for gas separation. J Memb Sci. 2010;364(1-2):263-277.

37. Zhou K, Chen X, Shao Z, Wan W, Biegler LT. Heterogeneous parallel method for mixed integer nonlinear programming. Comput Chem Eng. 2014;66:290-0300.

38. Ohs B, Lohaus J, Wessling M. Optimization of membrane based nitrogen removal from natural gas. J Memb Sci. 2016;498:291-301.

39. Kunde C, Kienle A. Global optimization of multistage binary separation networks. Chem Eng Process - Process Intensif. 2018; 131: 164-177.

40. Aliaga-Vicente A, Caballero JA, Fernandez-Torres MJ. Synthesis and optimization of membrane cascade for gas separation via mixed-integer nonlinear programming. AIChE J. 2017;63(6):1989-2006.

41. Nymeijer DC, Visser T, Assen R, Wessling M. Composite hollow fiber gas-liquid membrane contactors for olefin/paraffin separation. Sep Purif Technol. 2004;37(3):209-220.

42. Coker DT, Freeman BD, Fleming GK. Modeling multicomponent gas separation using hollow-fiber membrane contactors. AIChE J. 1998;44(6):1289-1302.

43. Gilassi S, Taghavi SM, Rodrigue D, Kaliaguine S. Simulation of gas separation using partial element stage cut modeling of hollow fiber membrane modules. AIChE J. 2018;64(5):1766-1777.

44. Pan CY. Gas separation by high-flux, asymmetric hollow-fiber membrane. AIChE J. 1986;32(12):2020-2027.

45. Marriott JI, Sørensen E, Bogle IDL. Detailed mathematical modeling of membrane modules. Comput Chem Eng. 2001;25:693–700.

46. Burns RL, Koros WJ. Defining the challenges for C3H6/C3H8 separation using polymeric membranes. J Memb Sci. 2003;211(2):299-309.

47. Spillman R. Economics of gas separation membrane processes. In: Noble RD, Stern SA, eds. Membrane Separations Technology. Principles and Applications. Amsterdam: Elsevier Science; 1995.

48. Baker RW, Wijmans JG. Two-stage membrane process and apparatus, US patents 5,256,295 and 5,256,296, 1993.

49.   Wijmans JG, Baker RW. The solution-diffusion model: a review. J Memb Sci. 1995;107(1-2):1-21.

50.   Luyben WL. Dynamic simulation of flooded condensers. Chem Eng Res Des. 2017;118:12-20.

51.   Zarca G, Urtiaga A, Biegler LT, Ortiz I. An optimization model for assessment of membrane-based post-combustion gas upcycling into hydrogen or syngas. J Memb Sci. 2018;563:83-92.

52.   Biegler LT, Grossmann IE, Westerberg AW. Systematic methods of chemical process design. Upper Saddle River, NJ: Prentice Hall; 1997.

53.   Alcántara-Avila JR, Gómez-Castro FI, Segovia-Hernández JG, Sotowa K-I, Horikawa T. Optimal design of cryogenic distillation columns with side heat pumps for the propylene/propane separation. Chem Eng Process - Process Intensif. 2014;82:112-122.
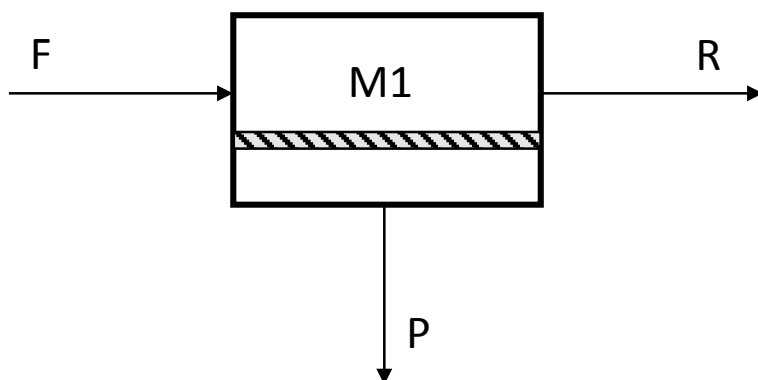
List of figure captions
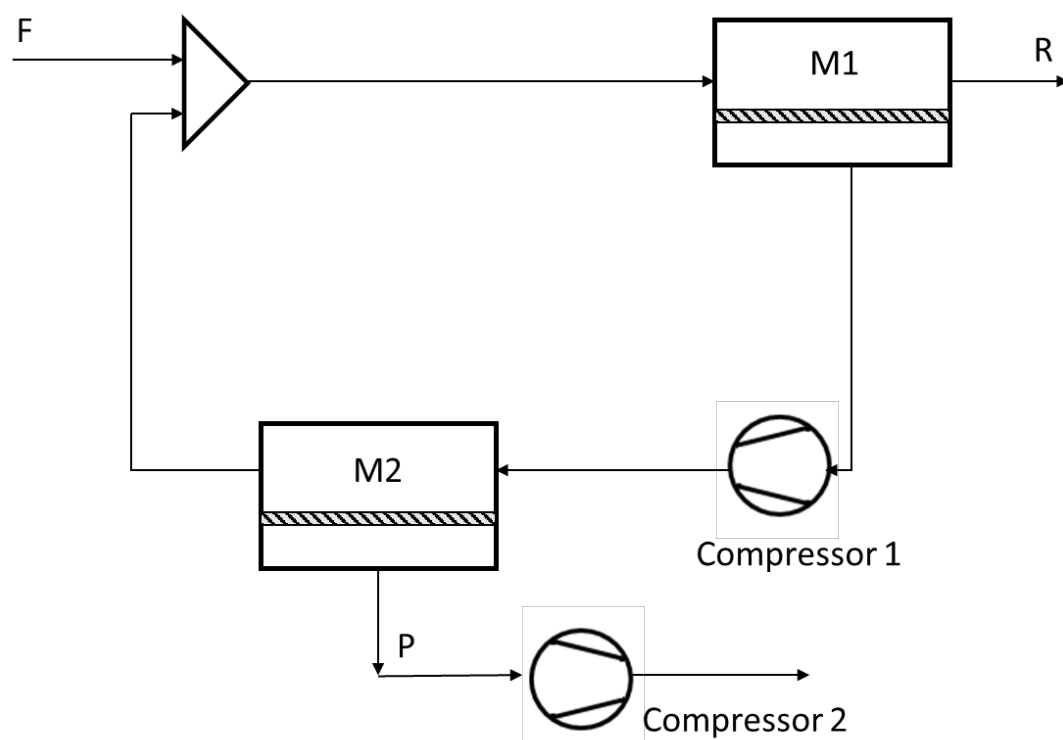
Figure 1. Single-stage membrane process.

Figure 2. Two-step membrane process.

Figure 3. Two-and-one-half membrane process.

Figure 4. Schematic diagram of the hollow fibers model.

Figure 5. Two stage process optimal design.

Figure 6. Propylene and propane transmembrane flux in stages M1 (A) and M2 (B) of the two stage process.

Figure 7. Propylene and propane molar fractions in the retentate and permeate streams of Stage 1 (M1).

Figure 8. Two-and-one-half stage process optimal design.

Figure 9. Propylene and propane transmembrane flux in stages M1 (A), M2 (B) and M3 (C) of the "two-and-one-half" stage process.

Figure 1. Single-stage membrane process.
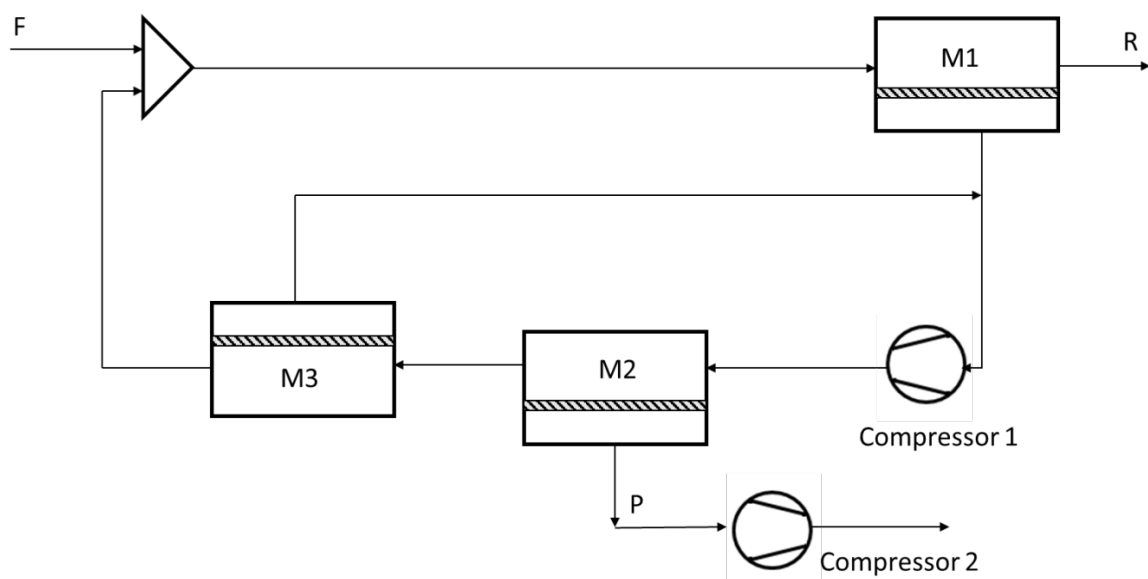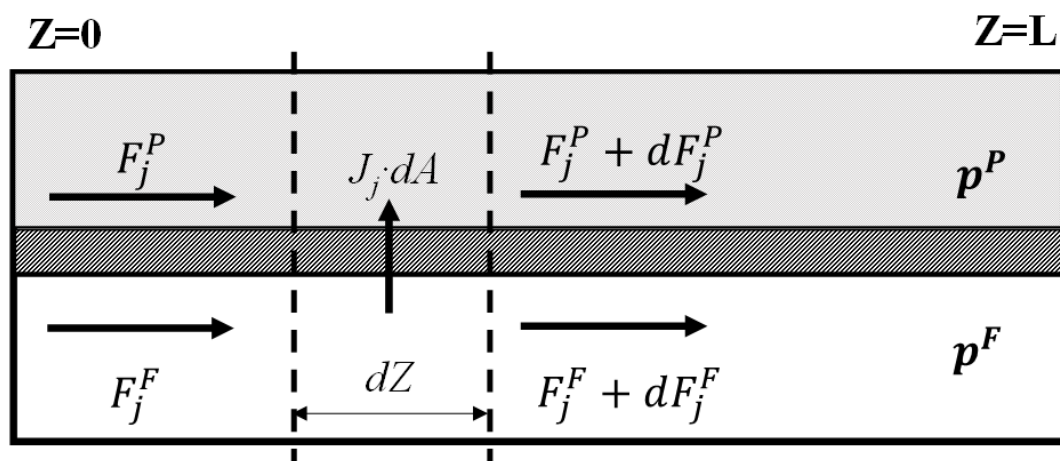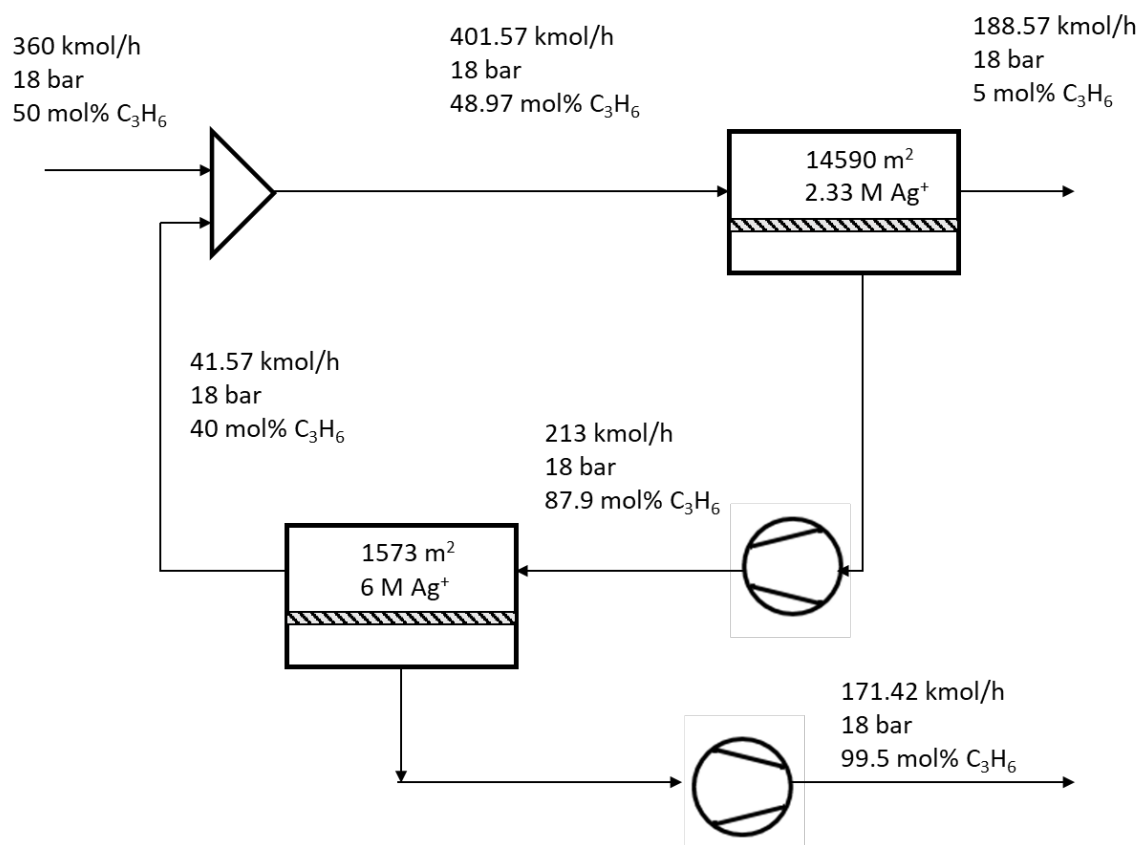
Figure 2. Two-step membrane process.

Figure 3. Two-and-one-half membrane process.

Figure 4. Schematic diagram of the hollow fibers model.

360 kmol/h
18 bar
50 mol% C_3H_6

401.57 kmol/h
18 bar
48.97 mol% C_3H_6

188.57 kmol/h
18 bar
5 mol% C_3H_6

14590 m^2
2.33 M Ag$^+$

41.57 kmol/h
18 bar
40 mol% C_3H_6

213 kmol/h
18 bar
87.9 mol% C_3H_6

1573 m^2
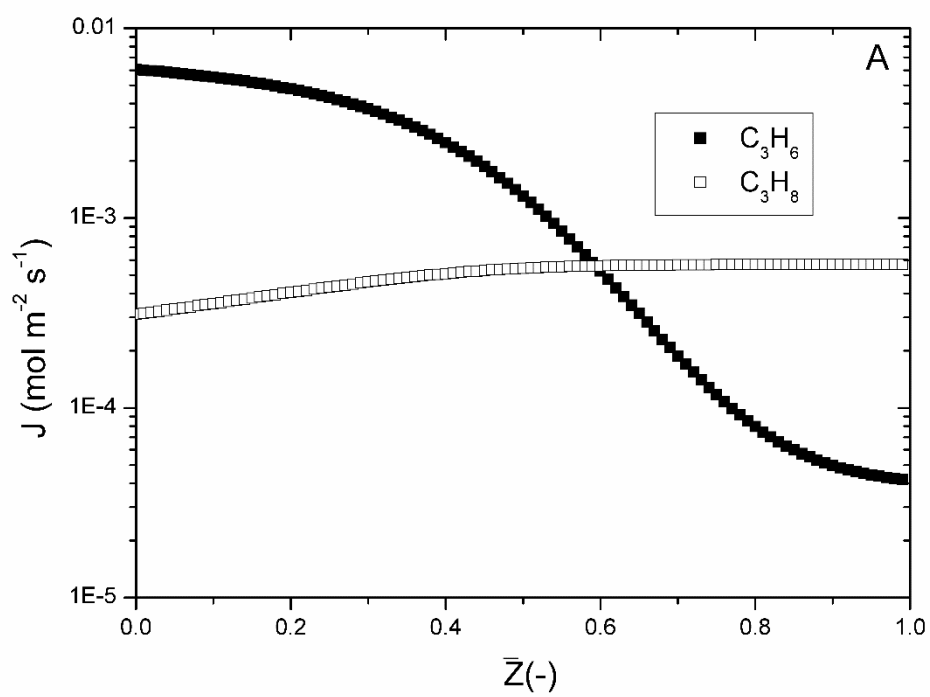6 M Ag$^+$

171.42 kmol/h
18 bar
99.5 mol% C_3H_6

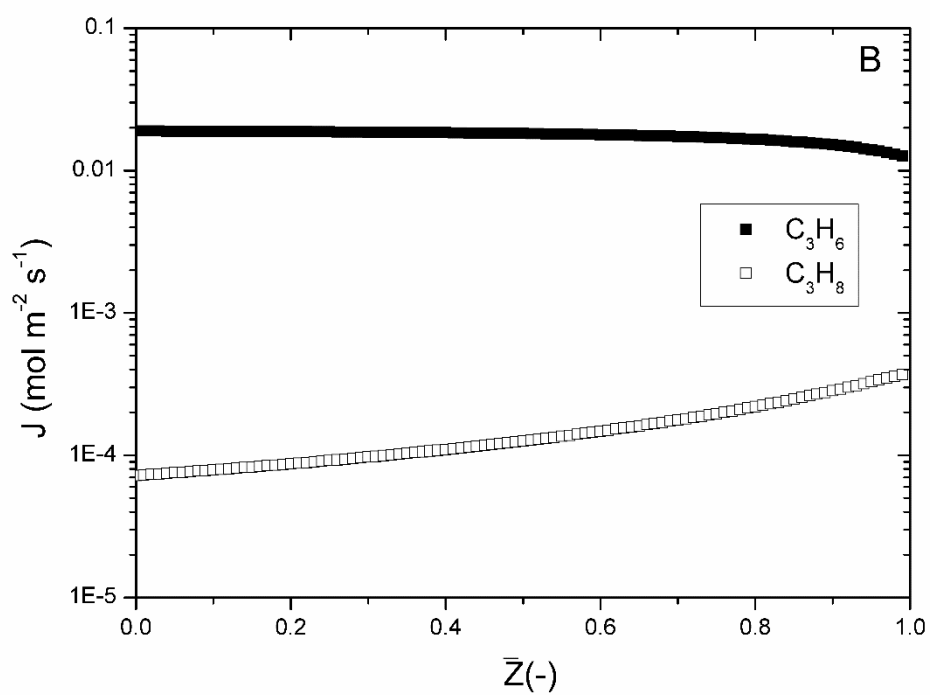*Figure 5. Two stage process optimal design.*

Figure 6. Propylene and propane transmembrane flux in stages M1 (A) and M2 (B) of
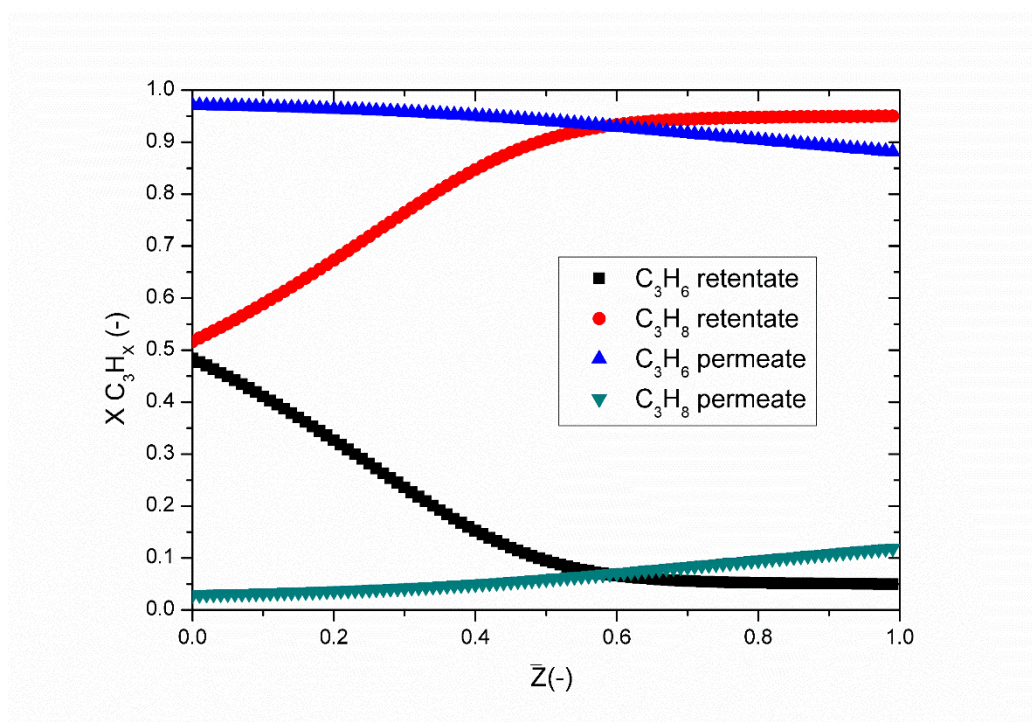
the two stage process.

Figure 7. Propylene and propane molar fractions in the retentate and permeate streams of Stage 1 (M1).
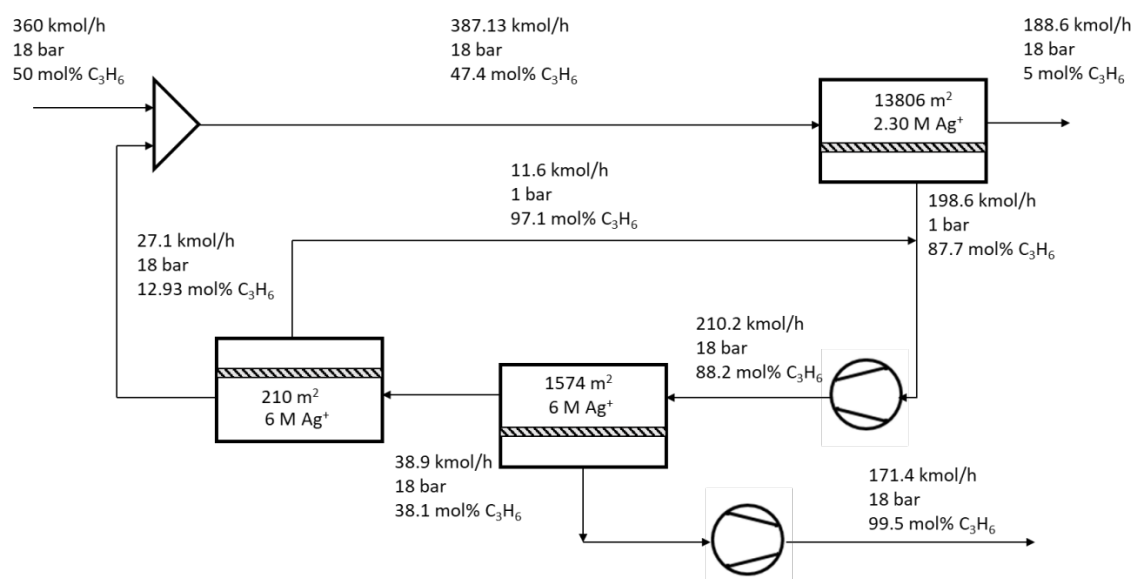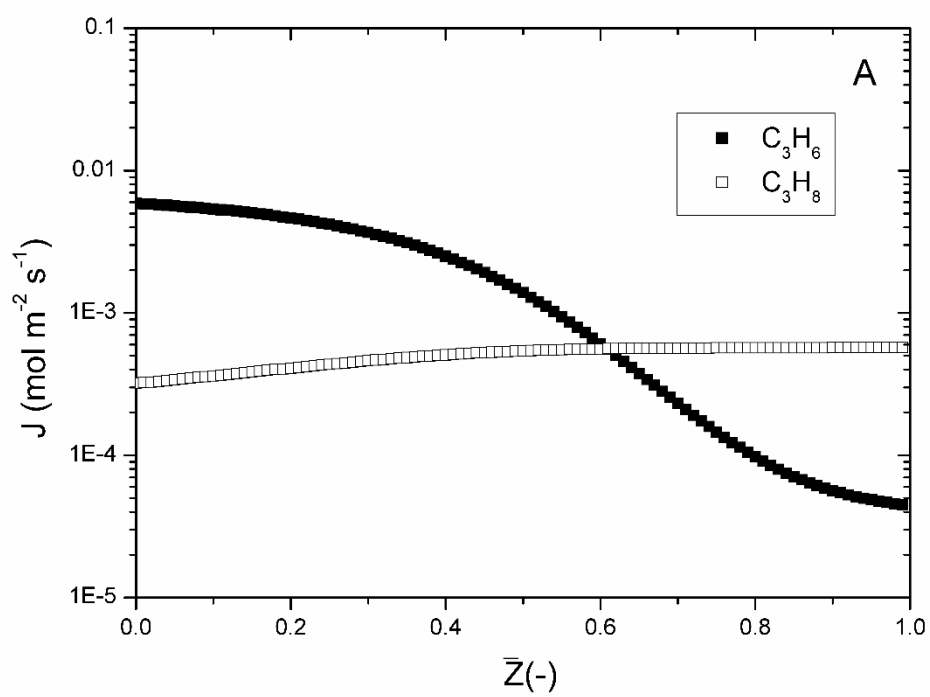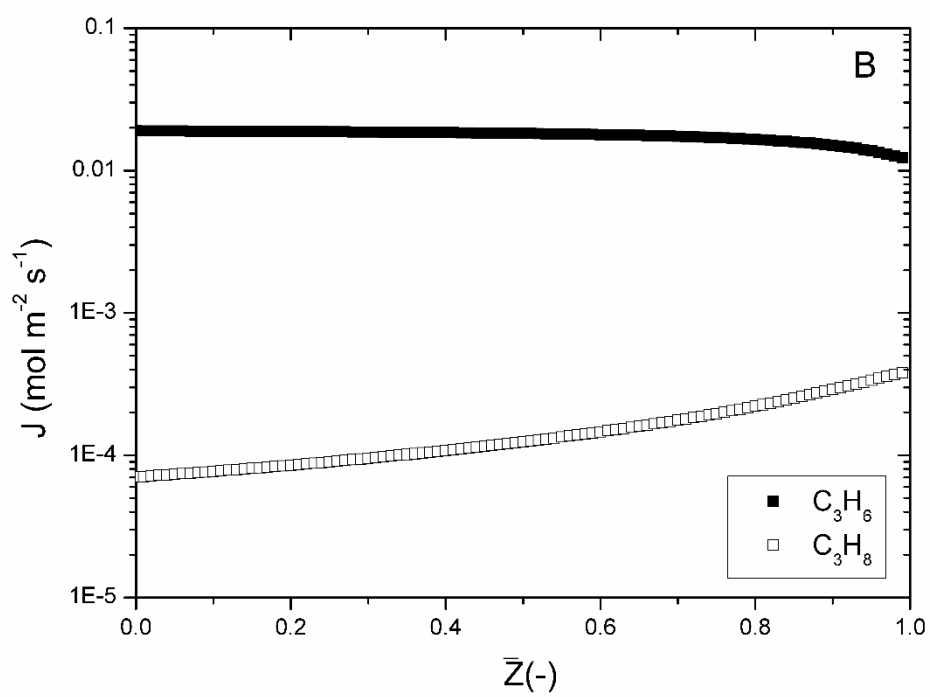
Figure 8. Two-and-one-half stage process optimal design.

Figure 9. Propylene and propane transmembrane flux in stages M1 (A), M2 (B) and M3

(C) of the "two-and-one-half" stage process.

List of Table captions

Table 1. Facilitated Transport Model Parameters at 323 K

Table 2. Process Feed Specifications, Parameters and Constraints

Table 3. Economic Evaluation Parameters

Table 4. Models Statistics

Table 5. Optimization Results of the Multistage Processes

Table 6. Multistage Processes Net Present Value Cost Compared to the Distillation Base
Case

Table 7. Multistage Processes Net Present Value Cost for 99.9% Propylene
Specification

Table 1. Facilitated transport model parameters at 323 K.

Parameter	Value	Reference
D_{comp} (x10^{11} m^2 s^{-1})	4.3	21
x_{IL} (-)	0.20	25
$H_{C_3H_6}$ (mol bar^{-1} m^{-3})	31.97	22
k_{eq} (m^3 mol^{-1})	0.17	22
α (x10^{11} m^2 mol^{-1} s^{-1})	2.37	25

Table 2. Process feed specifications, parameters and constraints.

Parameter	Value
Feed temperature (K)	323
Feed pressure (bar)	18
Feed flowrate (kmol h^{-1})	360
Feed composition (C_3H_6 mole frac.)	0.50
Permeate pressure (bar)	1-18
Required C_3H_6 purity (x_i)	≥ 0.995
Required C_3H_8 purity (x_i)	≥ 0.950
C_3H_8 permeability (Barrer) [a]	20
Membrane thickness (µm)	20
Silver loading[b] (mol l^{-1})	0-6

[a] 1 Barrer = 3.348×10^{-16} mol^3 m m^{-2} Pa^{-1} s^{-1}.

[b] Silver loading delimited according to the experimentally studied concentration range.[24,25]

Table 3. Economic evaluation parameters.

Parameter	Symbol	Value
Membrane		
Membrane replacement factor (%)	MR	10
Polymer load (g m^{-3})	PL	1.11×10^6
Ionic liquid load (g m^{-3})	ILL	2.76×10^5
Polymer cost ($ g^{-1})	PP	0.7
Ionic liquid cost ($ g^{-1})	ILP	0.8
Silver salt cost ($ g^{-1})	AGP	13.0
Compressors		
Compressor stages	N_{st}	3
Cost function exponent	a	0.77
Electricity price ($ kWh^{-1})	EP	0.15
Isentropic efficiency	η_c	0.70
Material and pressure factor	MPF	1
Compression ratio	Cr_{max}	2.62
Module factor	MF	3.11
Ratio of heat capacities	Υ	1.15
Reference cost ($)	C_0	23000
Reference size (kW)	S_0	74.57
Update factor	UF	4.71
Project		
Annual operation (h y^{-1})	OF	8000
Investment rate (%)	r	10
Period (y)	T_{inv}	15

Table 4. Models statistics

	Two-stages	Two-and-one-half stages
Number of single equations	4314	8122
Number of single variables	4321	8130

Table 5. Optimization results of the multistage processes

	Two Stages	Two-and-one-half Stages
Compressor power 1 (kW)	704	694
Compressor power 2 (kW)	563	563
M1 total area (m^2)	14590	13806
M2 total area (m^2)	1573	1574
M3 total area (m^2)	*n/a*	210
M1 carrier loading (M)	2.33	2.30
M2 carrier loading (M)	6	6
M3 carrier loading (M)	*n/a*	6
M1 membrane cost ($ m^{-2})	138	136
M2 membrane cost ($ m^{-2})	324	324
M3 membrane cost ($ m^{-2})	*n/a*	324
M1 permeate pressure (bar)	1	1
M2 permeate pressure (bar)	1	1
M3 permeate pressure (bar)	*n/a*	1
Compressors CAPEX (MM$)	4.49	4.47
Membrane CAPEX (MM$)	2.53	2.46
Compressors OPEX (MM$ yr^{-1})	1.51	1.51
Membrane OPEX (MM$ yr^{-1})	0.258	0.246

Table 6. Multistage processes Net Present Value Cost compared to the distillation base case.

	Distillation	Two Stages	"Two-and-one-half" Stages
OPEX (MM$ y^{-1})	4.1[a]	1.77	1.75
CAPEX (MM$)	8.9[b]	7.02	6.93
NPVC (MM$)	39.7	20.5	20.3

[a] based on the design parameters presented elsewhere.[29]

[b] calculated according to the "Guthrie's Modular Method for Costing and Sizing"[52]

Table 7. Multistage processes Net Present Value Cost for 99.9% propylene specification

	Propylene 99.5 %		Propylene 99.9 %	
	Two stages	"Two-and-one-half" stages	Two stages	"Two-and-one-half" stages
OPEX (MM$ y^{-1})	1.77	1.75	Not feasible	3.09
CAPEX (MM$)	7.02	6.93		10.6
NPVC (MM$)	20.5	20.3		34.09